AIChE WILEY InterScience DISCOVER SOMETHING GREAT

Bubble Velocity, Size, and Interfacial Area Measurements in a Bubble Column by Four-Point Optical Probe

Junli Xue, Muthanna Al-Dahhan, and M. P. Dudukovic
Chemical Reaction Engineering Laboratory (CREL), Washington University, St. Louis, MO 63130

R. F. Mudde
Kramers Laboratorium voor Fysische Technologie, Delft University of Technology, Delft, South Holland, Netherlands

DOI 10.1002/aic.11386
Published online December 10, 2007 in Wiley InterScience (www.interscience.wiley.com).

The four-point optical probe is applied in a bubble column with an air–water system to investigate the bubble properties (local gas holdup, velocity, chord length, specific interfacial area, and frequency) over a range of gas superficial velocities. Both bubbles moving upward and downward are recorded and measured as opposed to only upward bubbles measured and reported in other studies involving probes. The probe worked efficiently in both bubbly flow and highly churn-turbulent flow at very high superficial gas velocities. Bubble properties at the conditions of churn-turbulent flow are obtained and investigated for the first time. The changes in the bubble velocity distribution, bubble chord length distribution, and specific interfacial area with superficial gas velocity, sparger design, and with axial and radial positions in the column are discussed.
 AIChE J, 54: 350–363, 2008
Keywords: bubble column, bubble properties, four-point optical probe

Introduction

The knowledge of bubble properties, including bubble velocity, bubble size, gas holdup, and specific interfacial area, is of considerable importance for the proper design and operation of bubble columns. For example, bubble properties play key roles in determining the heat and mass transfer rate in bubble columns. Furthermore, bubble size distribution and bubble velocity distribution are key parameters in evaluating the drag forces on bubbles and in using the bubble population balance in computational fluid dynamics (CFD). However, because of the limitations of the commonly available measurement technique, important bubble properties in 3D bubble columns are scarce in the literature, especially in churn-turbulent flow, and the available data are often not reliable.[1] After validation of the measurements obtained by the four-point optical probe with digital camera in 2D calibration systems,[2] the probe was utilized over a range of operating conditions in a cylindrical bubble column, 6.4 in. (16.2 cm) in diameter, to determine the bubble velocity distribution, bubble chord length (the length of the chord that the probe tip passed by in the bubble) distribution, local gas holdup, and specific interfacial area. The operating conditions were the same as those used for the γ ray computed tomography (CT) and computer automated radioactive particle tracking (CARPT) experiments conducted by Ong.[3] At the operating conditions used (superficial gas velocity from 2 to 60 cm/s, pressure from 0.1 to 1.0 MPa), the two-phase flow in the bubble column changes from bubbly flow to highly churn-turbulent flow. Bubble properties, such as chord length distribution and velocity distribution locally at various positions in the column, at the conditions of higher gas superficial velocities were measured for the first time, and present new data needed for CFD validation and engineering model

Correspondence concerning this article should be addressed to M. P. Dudukovic at dudu@wustl.edu.

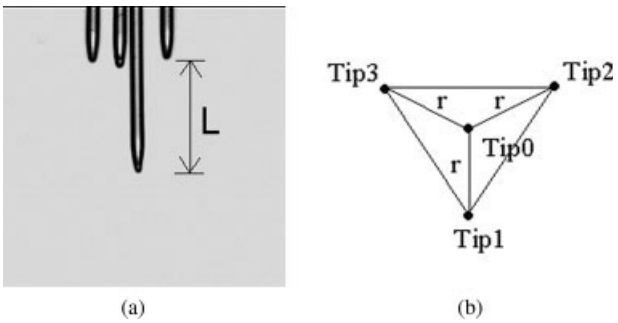

Figure 1. Configuration of the four-point optical probe.

(a) Side view; (b) Bottom view.

development. In addition, both upward and downward bubbles have been measured for the first time instead of only measuring upward bubbles as reported in previous studies using probes. Furthermore, the profile of the specific interfacial area as a function of column radial position at different axial elevations has been measured by the four-point optical probe readily and reliably.

Experimental Setup

The configuration of the four-point optical probe, which was made in-house, was shown in Figure 1. Three of the four tips of the probe are of the same length and form an equilateral triangle. The fourth, central tip is positioned through the inertial center of this triangle, and is about 2.0 mm longer than the others. The radial distance from the central fiber to each of the others that surround it is about 0.6 mm. Hence, the diameter of the four-point probe is about 1.2 mm. The tip of the glass fibers is shaped into a cone or semisphere. This shape assures that most light is reflected at the fiber tip when the probe is in gas phase and is scattered at the probe tip when it is in the liquid phase, due to the difference in the refractive index between the glass, the liquid phase, and the gas phase. By transferring the reflected light into voltage, the probe can generate a response (as shown in Figure 2) to each bubble that hits the probe tip. Then the bubble properties (local gas holdup, velocity, chord length, specific interfacial area, and frequency) can be derived by processing the response with an appropriate algorithm. The bubble properties by the four-point probe have been validated against imaging method in a 2D transparent bubble column. More details about the probe can be found in the preceding paper[1] and in the thesis of Xue.[2]

The configuration of the 16.2-cm (6.4 in.) diameter stainless steel bubble column is shown in Figure 3. In this figure also the four-point probe locations at which measurements were made are schematically presented. The setup was operated in the batch mode regarding the liquid, with tap water as the liquid phase. For the gas phase, filtered, dry compressed air was used.

The four-point probe measurements were conducted at different gas velocities and pressures. The operating conditions employed are listed in Table 1. Three axial measuring positions, that is, $z/D = 1.7$, 5.1, and 8.5, and seven radial positions, that is, $r/R = \pm 0.9$, $r/R = \pm 0.6$, $r/R = \pm 0.3$, and $r/R = 0$ were used, where positive and negative values of r/R represent different locations along the diameter of the column (Figure 3). The optical probe must employ the fixed ports available on the column wall. Because of this physical limitation of the column, that is, the ports are all located on the same vertical plane (Figure 3), the radial measuring positions at each axial position are along one column diameter and all the measuring positions were in one single vertical plane in the column (i.e., the full azimuthal dependence was not investigated). The configuration of the spargers used is shown in Figure 4 and Table 2.

The operating principle of the four-point probe[1,2] ensures that it accurately measures bubbles moving upward when it is positioned with tube tips facing downward. To capture downward moving bubbles, the probe is positioned with the tips facing upward. Visual observations indicate that, at high gas superficial velocity, many bubbles move downward in bubble columns in transition flow and churn-turbulent flow, especially in the wall zone. Hence, the four-point probe was positioned in two directions at each measuring site, that is, upward and downward, and in both cases the probe tip was positioned at the same point (Figure 3). In this way, both bubbles moving upward and those moving downward can be measured, instead of only bubbles moving upward as usually done in other reported studies involving probes.

Results and Discussion

The effect of superficial gas velocity on bubble properties

The superficial gas velocity, U_g, is one of the key operating variables that affect the hydrodynamics in bubble columns, including bubble properties. Figure 5a shows, for Sparger 2, the radial profiles of the local gas holdup, $\varepsilon_{g,l}$, at different U_g and the changes of $\varepsilon_{g,l}$ with U_g at different radial positions. The error bars, which come from the standard deviation of replicated measurements, are also displayed. It is clear from Figure 5a that at $U_g = 2$ cm/s, which is bubbly flow, the radial profile of the local gas holdup is flat (only in the core flow, that is, r/R from -0.9 to 0.9, not include the very near wall zone, this also applies to the following discussion). The local gas holdup profile is parabolic in shape when U_g is larger than 8 cm/s, when the flow changes from transition flow to churn-turbulent flow. Furthermore, the

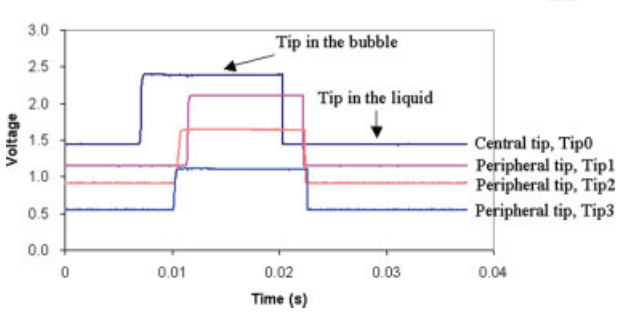

Figure 2. Response of the four-point probe to a bubble pierced through.

[Color figure can be viewed in the online issue, which is available at www.interscience.wiley.com.]

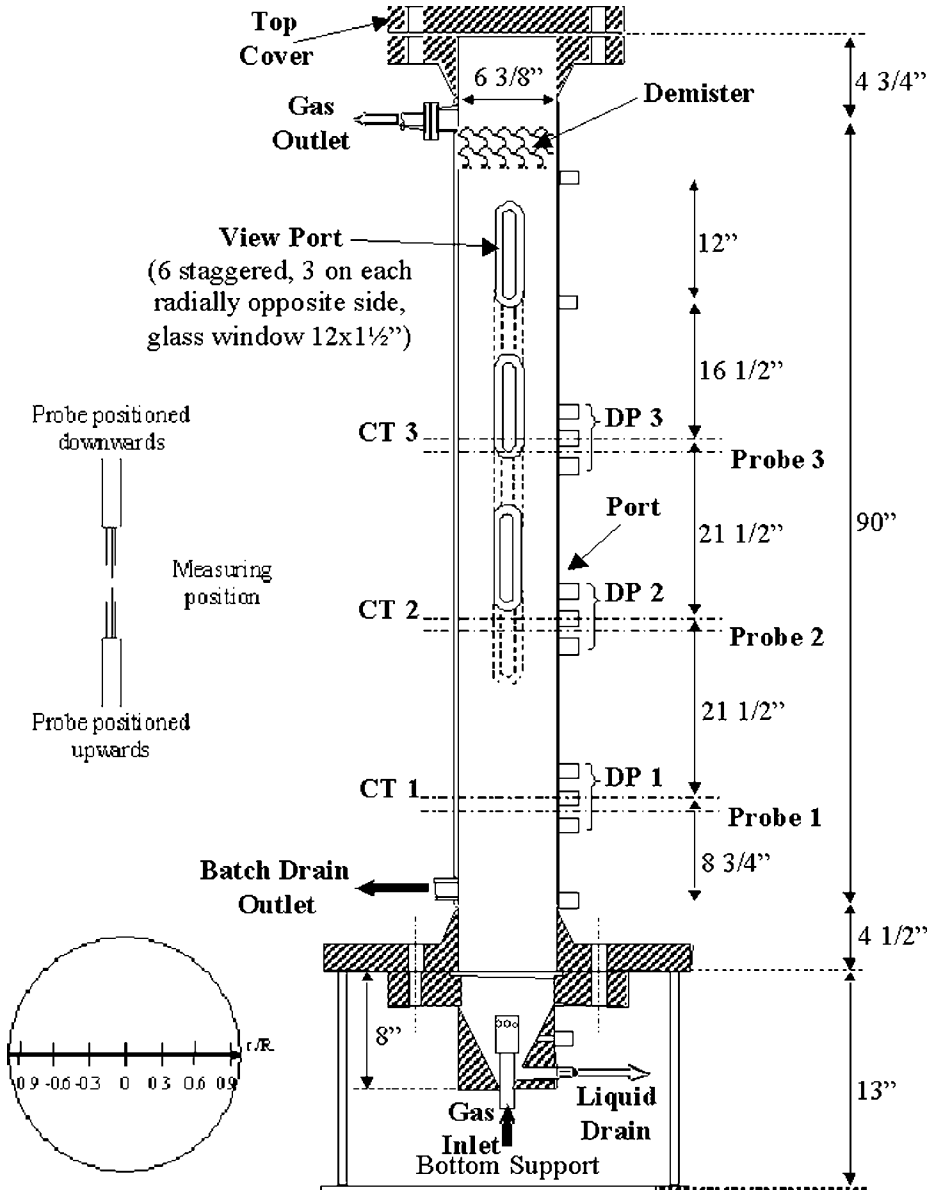

Figure 3. The configuration of the bubble column.

higher the gas velocity, the steeper the parabolic-like gas holdup radial profile. These observations are corroborated with the CT experimental results.[3,4] It is also noted that the measured bubble properties are not strictly symmetric in the horizontal direction in the plane of measurement. Visual observation through the windows on the column wall is also indicative of the asymmetry of the flow in the column. Possible causes for this asymmetry include the possibility that the bubble column is not vertical (which is not true in this study because the column was adjusted to be vertical by hanging hammer), that the sparger used is not axially symmetric, and that the coherent structure in the flow is nonsymmetric.[5] One should note that while we talk about radial profiles in this manuscript, these are not azimuthally averaged values as we normally report from our tomography measurements, but values obtained in a single vertical plane that passes through the central axis of the column. Whether azimuthal averaging would make these profiles seem more symmetric is not known since such measurements, due to the previously explained limitations of the column, were not made in this study.

It is found that the radial profiles of both specific interfacial area (Figure 5b) and bubble frequency (the number of bubbles that hit the central tip of the probe per second) and their changes with U_g are similar to the radial profile of the local gas holdup. The similarity between these profiles is the result of the fact that local gas holdup, specific interfacial area, and bubble frequency are strongly correlated. Speaking generally, an increase in bubble frequency leads to an increase in gas holdup and specific interfacial area.[6]

The radial profiles of the mean bubble velocity, $\bar{v}_b$, at different U_g are shown in Figure 6. Positive values of the bub-

Table 1. Column Dimensions and Selected Operating Conditions

Column ID, D (cm) (in.)	16.26 (6.4 in.)
Temperature (°C)	20
Pressure (MPa)	0.1
Dynamic liquid height (cm) (in.)	180 (70.9 in)
Probe vertical measurement levels from the distributors, z (cm) (in.)	27.7 (10.9), 82.3 (32.4), 136.9 (53.9)
z/D	1.7, 5.1, 8.5
Probe radial measuring positions (r/R)	±0.9, ±0.6, ±0.3, 0
Liquid (Tap water)	Batch
Gas (Air)	Continuous

Detailed Operating Conditions for Each Gas Distributor

Sparger	Pressure (MPa)	U_g (cm/s)
No. 1 Cross sparger (open area 0.1%)	0.1	30
No. 2 Perforated plate (0.15%)	0.1	2, 8, 14, 30, 45, 60
No. 3 Perforated plate (1.0%)	0.1, 0.4, 1.0	30

ble velocity mean that bubbles move upward, while the negative values mean that bubbles move downward. As expected, the radial profile of $\bar{v}_b$ is flat at $U_g = 2$ cm/s, which is bubbly flow, and it is almost parabolic when U_g is larger than 8 cm/s, when the flow changes to transition flow and churn-turbulent flow (Figure 6a). Note that the average bubble velocity for $U_g = 2$ cm/s is in agreement with the reduction of the bubble slip velocity in a swarm as predicted by the Richardson and Zaki correlation $v_s/v_\infty = (1 - \varepsilon_g)^n$, with $n = 2.4$ and v_∞, the terminal velocity of a single bubble, ~25 cm/s. Figure 6b shows that $\bar{v}_b$ was always positive and increased with U_g in the core of the column, and the rate of increase in $\bar{v}_b$ with U_g in the bubbly flow regime was faster than in the churn-turbulent flow regime. In the wall zone ($r/R = \pm 0.9$), $\bar{v}_b$ was positive in bubbly flow ($U_g = 2$ cm/s) and was small or even negative at $U_g > 8$ cm/s. Above U_g of 14 cm/s, the magnitude of $\bar{v}_b$ increased slowly with U_g. In the range of U_g investigated ($U_g = 2$–60 cm/s), the minimum $\bar{v}_b$ was detected in the wall zone at $U_g = 8$ cm/s, in the transition regime from bubbly flow to churn-turbulent flow.

The bubble velocity distribution in the wall zone (Figure 7, $r/R = \pm 0.9$, $z/D = 5.1$) obtained by the four-point optical probe clarifies the observed behavior of the mean bubble velocity, $\bar{v}_b$. It should be noted that a large portion of bubbles of very low velocity can not be measured by the probe. This is because it takes a relatively long time for very slow bubbles to pass through the four tips of the probe. During this time interval, if the flow field around the bubble changes, the bubble velocity also changes during its passage by the probe since bubbles move with the liquid flow. In this case, the velocity of the bubble determined by the four-point probe is the mean of the early slow velocity and the later high velocity. Hence, the four-point probe tends to underestimate the probability of bubbles of very low velocity. However, it should be noted that this bias is usually not significant because the vertical distance between the central tip and the other tips of the probe is about 2 mm. Hence, for assumption, if the time scale of the flow field change is 0.1 s, then only bubbles with velocity lower than about 2 cm/s will be affected. It should be noted that any measurement technique that uses "time of flight" has a bias for measuring velocities close to zero in a fluctuating flow. Usually the percentage of bubbles with such low velocity for which the bias affects the results is small but not always. The bias happens both for bubbles moving upward and downward, and hence, the mean bubble velocity is not affected much by this bias.

At $U_g = 2$ cm/s, all bubbles move upward (Figure 7a), and the peak in the bubble velocity distribution is thin and sharp. At $U_g > 8$ cm/s, the bubble velocity distributions at $r/R = -0.9$ and $r/R = 0.9$ are different. At $r/R = -0.9$, more bubbles move downward than upward while at $r/R = 0.9$, almost as many bubbles move upward as downward. As a result, the radial profile of $\bar{v}_b$ is not symmetric at $z/D = 5.1$ and $\bar{v}_b$ at $r/R = -0.9$ is smaller than that at $r/R = 0.9$ (Figure 6a). When U_g increased from 8 to 14 cm/s (i.e., in the transition flow regime), the mean velocity of bubbles moving upward increases greatly (from 9.45 to 20.9 cm/s at $r/R = -0.9$ and 12.4 to 28.3 cm/s at $r/R = 0.9$) whereas that of bubbles moving downward increases mildly in magnitude (from −33.8 to −39.1 cm/s at $r/R = -0.9$ and −28.2 to −34.6 cm/s at $r/R = 0.9$). This is because large bubbles,

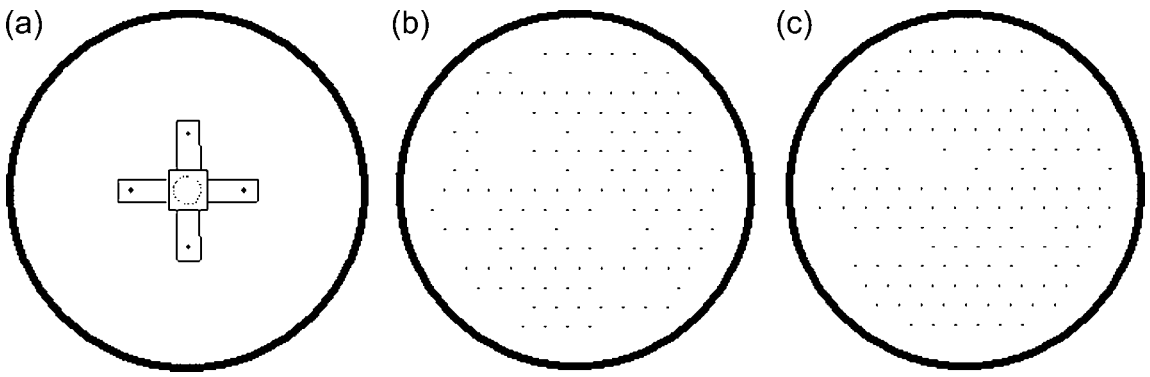

Figure 4. Schematic of the sparger configurations.

(a) No. 1 cross sparger, (b) No. 2 uniform perforated plate (small hole), (c) No. 3 uniform perforated plate (large hole, shown not to scale).

Table 2. Specifications of the Sparger Configurations

Sparger (No.)	Number of Holes (N_H)	Diameter of Holes (D_H) (mm)	Hole Pattern	Open Area (%)
1	4	2.54	25.4 mm off center, facing downwards	0.100
2	163	0.50	10-mm triangle pitch	0.156
3	163	1.32	10-mm triangle pitch	1.09

which have high velocity, arose in the transition flow regime and assembled in the central stream of the column (this is evident from an increase in the number of bubbles of high velocity in the bubble velocity distributions at $U_g = 8$ and 14 cm/s, Figures 8b, c). The velocity of bubbles moving downward in the wall zone increased mainly due to the enhancement of the liquid recirculation. Hence, the velocity of bubbles moving upward jumped and of bubbles moving downward increases only mildly in the transition flow regime. In churn-turbulent flow, at $U_g > 14$ cm/s, the percentage of bubbles moving downward in the wall zone increased slowly with U_g.

The bubble velocity distributions in the center of the bubble column ($r/R = 0$, $z/D = 5.1$) at different U_g are shown in Figure 8. In contrast to the bubble velocity distribution in the wall zone, most bubbles move upward in the column center. The percentage of bubbles moving downward increased with U_g, but even at very high gas velocity, for example, $U_g = 60$ cm/s, only a small percentage of bubbles moved downward in the column center. Bubbles moving downward in the column center include small bubbles that exist in the wakes of large bubbles. This may be due to the chaotic nature of the flow in bubble column where the flow reversal occurs even in churn-turbulent flow, dragging bubbles downward. In churn-turbulent flow, the number of large bubbles increases with U_g and liquid recirculation is enhanced.[3] Hence, there are more bubbles moving downward being detected by the four-point probe. The bubble velocity distribution in the column center spreads more widely with increased U_g, and the magnitude of the mean velocity of bubbles moving upward is much larger than that of bubbles moving downward.

The bubble chord length distributions obtained by the four-point optical probe at different gas velocities in the wall zone at $r/R = -0.9$ (the shape of bubble chord length distributions at $r/R = 0.9$ are similar to that at $r/R = -0.9$) and in the center of the column ($r/R = 0$) are displayed in Figure 9. At the column center ($r/R = 0$), the number of bubbles used for the calculation of the bubble chord length distribution is over 10,000 at $U_g \geq 8$ cm/s and about 4000 at $U_g = 2$ cm/s. In the wall region ($r/R = -0.9$), the number is over 5000 and about 4000 at the above two gas superficial velocities, respectively. The large number of bubbles for the derivation of the bubble chord length distribution and mean bubble chord length ensures statistically representative results. It can be seen that in the column center the probability of both small and large chord lengths increases with increased U_g, and the spread of the bubble chord length distribution is wider (Figure 9a). Note that at $U_g = 8$ cm/s the median of the pdf seems to be located at the highest chord length. In the wall zone (Figure 9b), the shape of the bubble chord length distribution does not change much with U_g when $U_g \geq 8$ cm/s. The probability of small bubble chord length increases with U_g, while that of large bubble chord length does not change much with U_g. This may be because large bubbles pass through the bubble column in the central bubble stream, as described by Chen et al.,[7] and seldom move into the wall zone, while small bubbles tend to enter the wall zone and move with the downward liquid flow.

The mean bubble chord length and the standard deviation of the bubble chord length distributions are plotted in Figure 10. The error bar for the mean bubble chord length is also shown. It can be seen that the mean and standard deviation of the bubble chord length distribution in the column center are almost identical to those in the wall zone at $U_g = 2$ cm/s, where the central stream of large bubbles does not

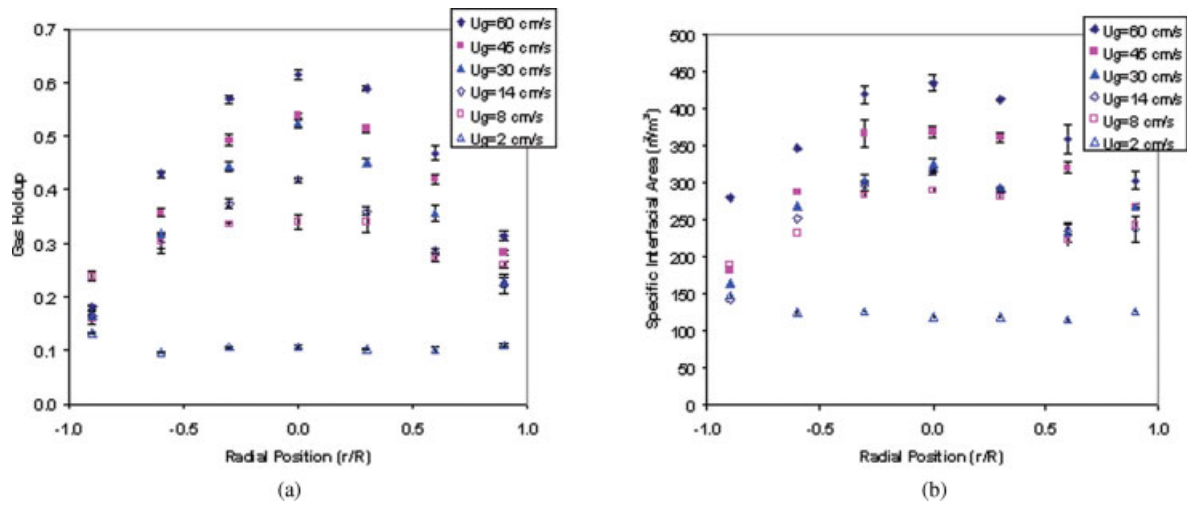

Figure 5. The radial profile of (a) local gas holdup and (b) specific interfacial area (Sparger No. 2, $z/D = 5.1$).

[Color figure can be viewed in the online issue, which is available at www.interscience.wiley.com.]

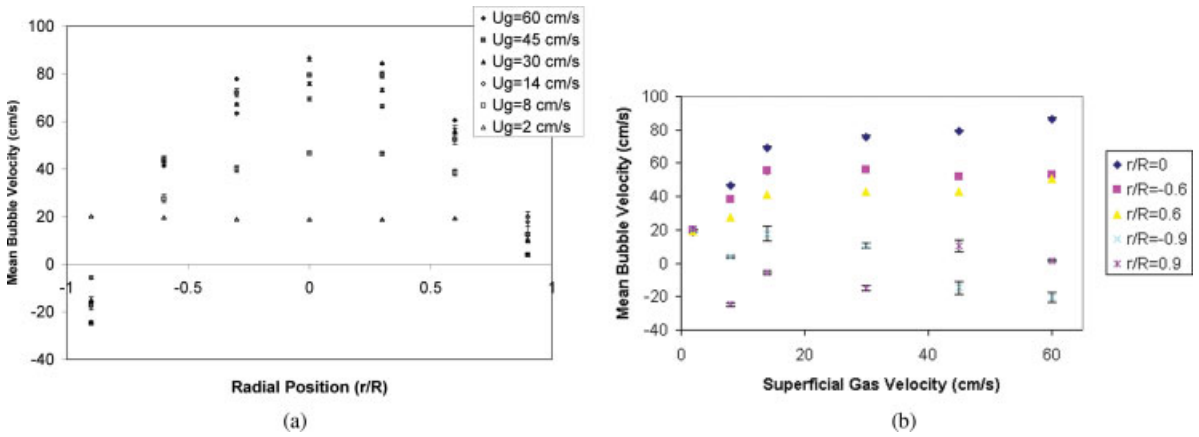

Figure 6. The (a) radial profile of mean bubble velocity and (b) its change with U_g (Sparger No. 2, z/D = 5.1) (positive values mean bubbles moving upward and negative values mean bubbles moving downward).

[Color figure can be viewed in the online issue, which is available at www.interscience.wiley.com.]

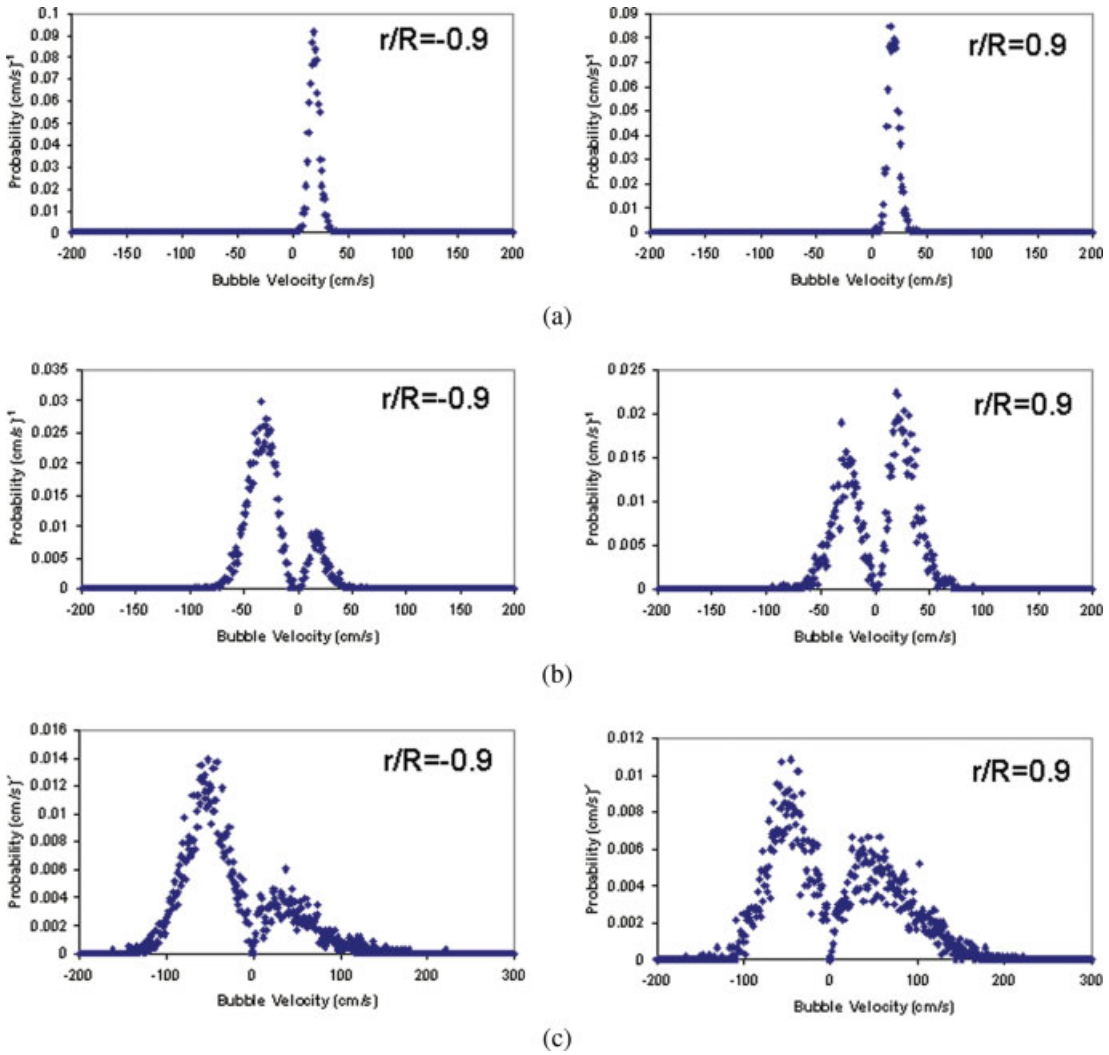

Figure 7. Bubble velocity distribution in the wall region at different superficial gas velocities (z/D = 5.1, Sparger No. 2).

(a) U_g = 2 cm/s; (b) U_g = 8 cm/s; (c) U_g = 60 cm/s. [Color figure can be viewed in the online issue, which is available at www.interscience.wiley.com.]

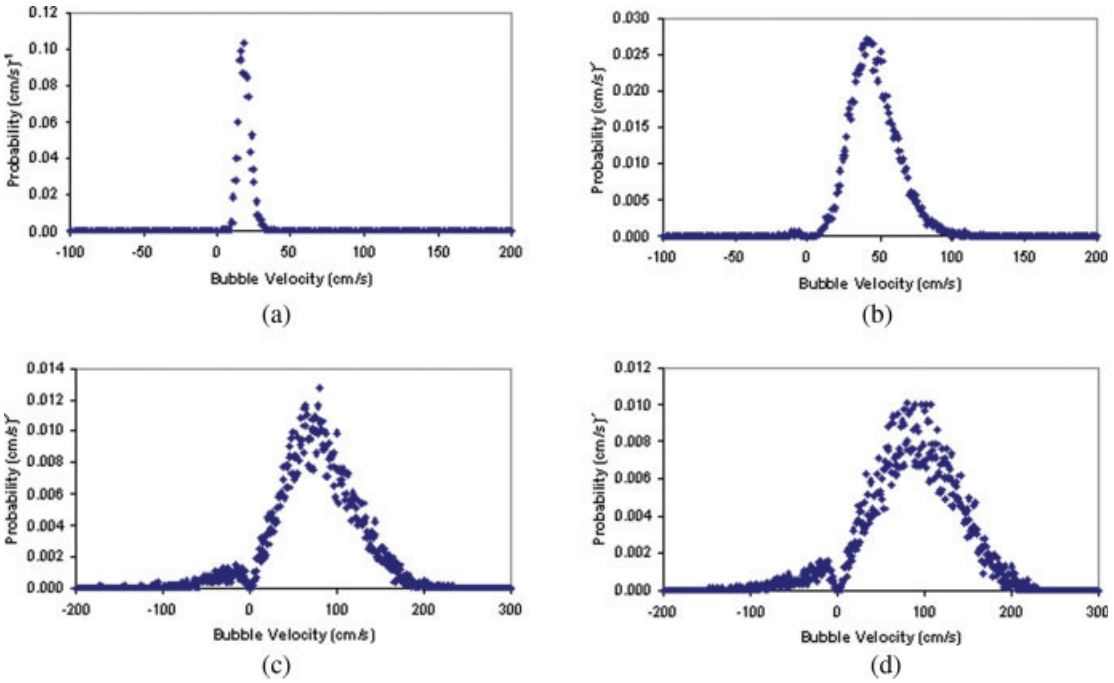

Figure 8. Bubble velocity distribution at different superficial gas velocities ($r/R = 0$, $z/D = 5.1$, Sparger No. 2).

(a) $U_g = 2$ cm/s; (b) $U_g = 8$ cm/s; (c) $U_g = 14$ cm/s; (d) $U_g = 60$ cm/s. [Color figure can be viewed in the online issue, which is available at www.interscience.wiley.com.]

exist, and at $U_g = 8$ cm/s, where the liquid recirculation is present, however, the number of large bubbles in the central stream is still small. This is in agreement with the findings of Mudde et al.[8] and of Mudde and Saito[9] who reported significant liquid circulation for the range of $U_g \sim 2$ to 6 cm/s. When $U_g \geq 14$ cm/s, the mean and standard deviation of the bubble chord length distribution in the column center are much larger than those in the wall zone due to the assembly of large bubbles in the central bubble stream. In the column center, the mean bubble chord length increases with U_g when $U_g \leq 30$ cm/s and decreases slightly with U_g when $U_g \geq 30$ cm/s (Figure 10a); the standard deviation increases quickly between $U_g = 8$ cm/s and $U_g = 30$ cm/s and decreases slightly with U_g when $U_g \geq 30$ cm/s. This is because in the transition flow regime and churn-turbulent flow regime, bubbles break and coalesce, and the number of both large and small bubbles increases and the bubble size distribution spreads wider than the relatively uniform bubble size distribution in bubbly flow. In the churn-turbulent flow regime, the increase in the number of small bubbles is faster than that of large bubbles, and hence, the mean bubble chord length decreases slightly with U_g. In the wall zone, the mean

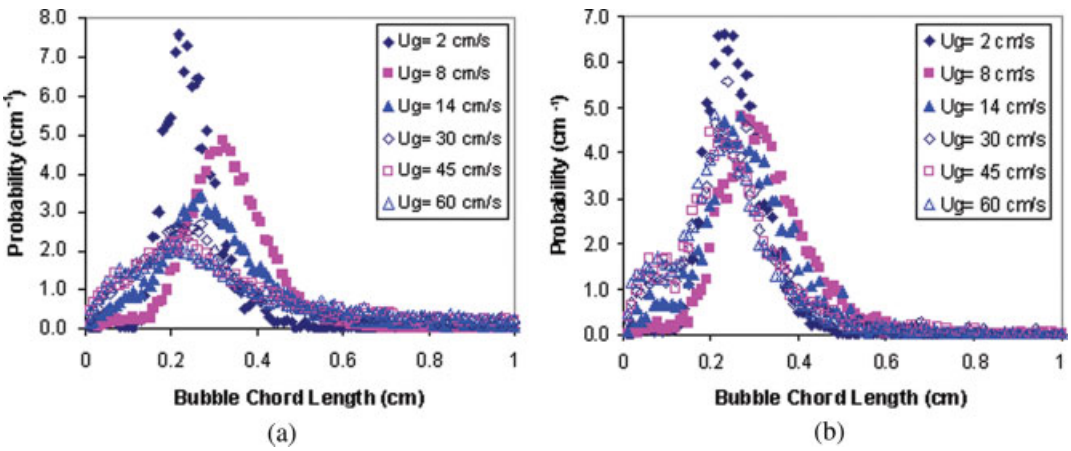

Figure 9. Bubble chord length distribution at different superficial gas velocities (Sparger No. 2, $z/D = 5.1$).

(a) $r/R = 0$; (b) $r/R = -0.9$. [Color figure can be viewed in the online issue, which is available at www.interscience.wiley.com.]

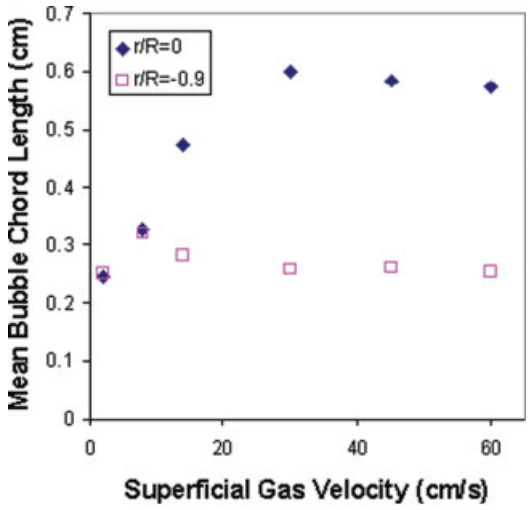

Figure 10. The (a) mean and (b) standard deviation of the bubble chord length distribution at different superficial gas velocities.

[Color figure can be viewed in the online issue, which is available at www.interscience.wiley.com.]

bubble chord length increases with U_g when $U_g \leq 8$ cm/s and decreases somewhat with U_g when $U_g \geq 8$ cm/s. The standard deviation keeps increasing with U_g in the range $U_g = 2$–60 cm/s, but the rate of increase is much slower than that in the column center. This is also the consequence of the fact that the large bubbles gather in the column center, and mainly small bubbles exist in the wall zone of the column.

Figure 11 shows the bubble velocity distribution and bubble chord length distribution at radial position $r/R = 0$, -0.3, -0.6, and -0.9. Because of the observation that the shape of the distributions at symmetric radial positions, for example, $r/R = 0.3$ and $r/R = -0.3$, are approximate to each other, the following discussions are valid for both sides in the column. It can be seen from Figure 11a that the percentage of bubbles moving downward increases from the column center to the wall zone; in the core of the column the change is slow, and bubbles moving upward are in the majority, whereas in the wall zone bubbles moving downward predominate. Since bubbles move with the liquid flow, this phenomenon is corroborated by research findings on liquid recirculation in bubble columns, which shows that the transition from upflow to downflow for the liquid recirculation happens at $r/R = 0.6$–0.7.[3] As shown in Figure 11b, the bubble chord length distributions in the core of the column are alike in shape. A sudden change happens within the wall zone where the percentage of small bubble chord lengths

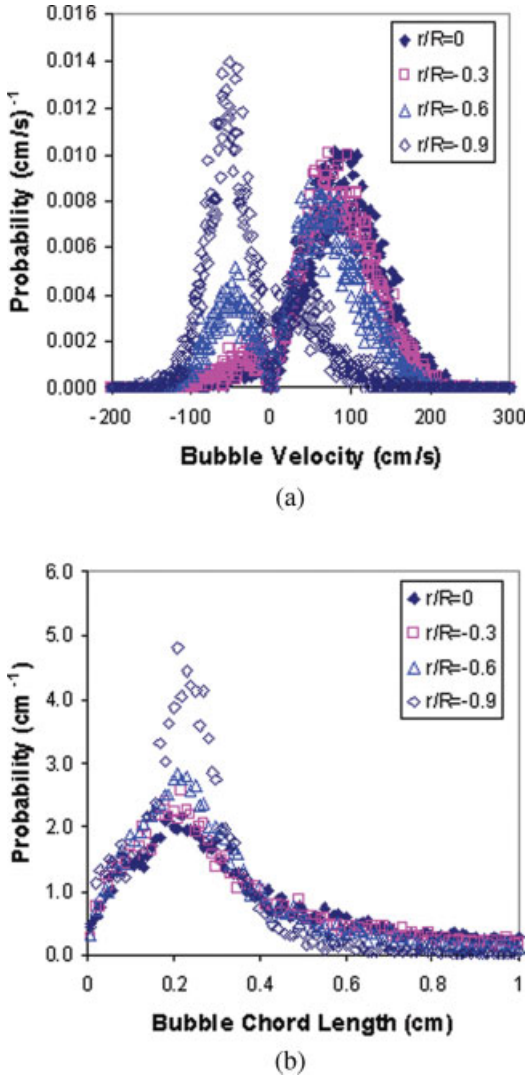

Figure 11. (a) Bubble velocity and (b) bubble chord length distribution at different radial positions (Sparger No. 2, U_g = 60 cm/s, z/D = 5.1).

[Color figure can be viewed in the online issue, which is available at www.interscience.wiley.com.]

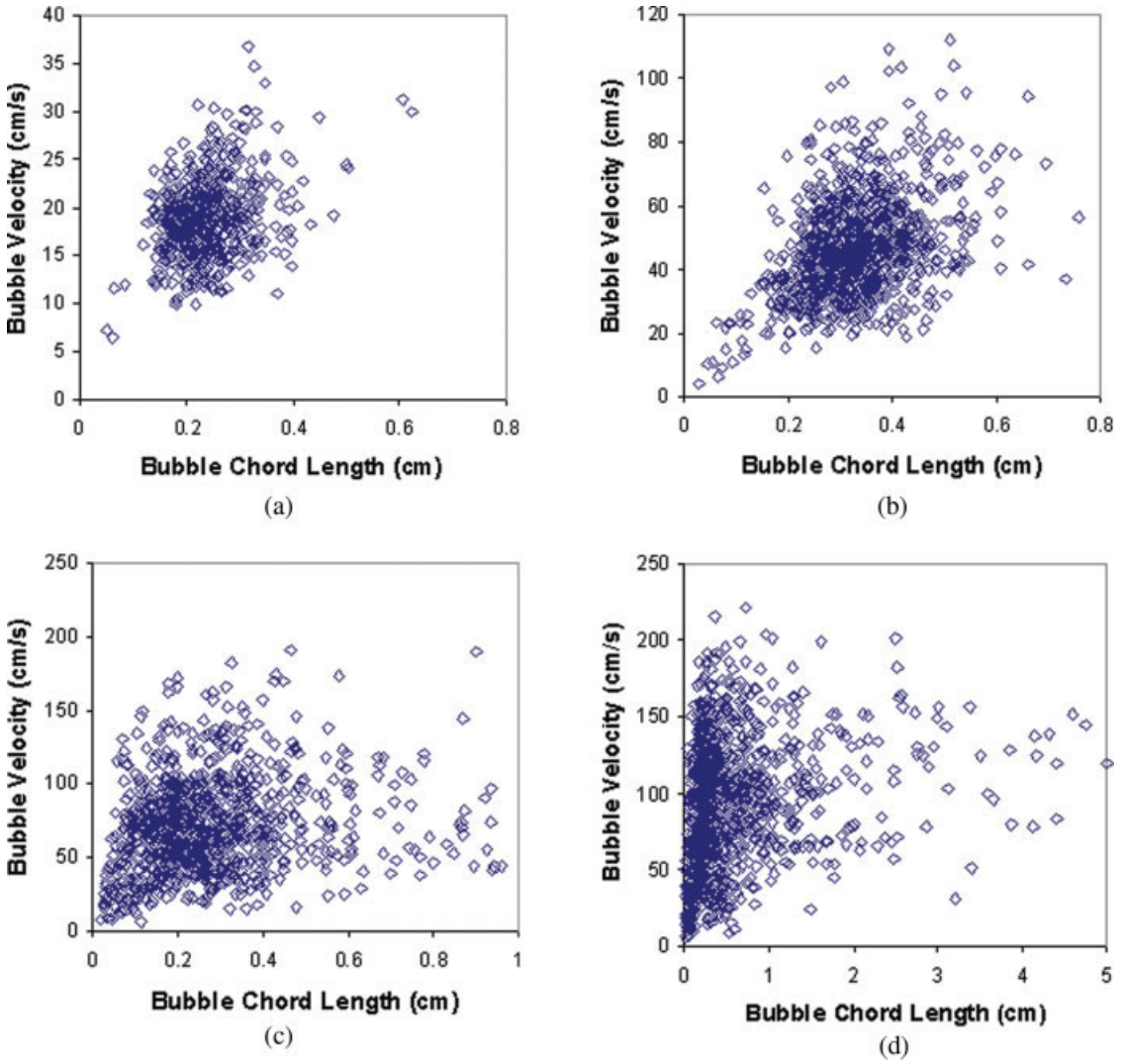

Figure 12. Bubble velocity vs. bubble chord length ($z/D = 5.1$, $r/R = 0$).

(a) $U_g = 2$ cm/s; (b) $U_g = 8$ cm/s; (c) $U_g = 14$ cm/s; (d) $U_g = 60$ cm/s. [Color figure can be viewed in the online issue, which is available at www.interscience.wiley.com.]

increases greatly because mainly small bubbles exist in the wall zone of the column. Hence, it can be concluded that in churn-turbulent flow in the core of the column ($r/R < 0.6$ in this study) the shape of the bubble velocity and bubble chord length distributions are alike, while in the wall zone they are very different from those in the core of the column.

Figure 12 shows the relationship between the bubble velocity and the bubble chord length in the center of the column at different U_g. It should be noted that the bubble velocity is the sum of the liquid velocity and the bubble's slip velocity since bubbles move with the liquid flow in bubble columns. In other words, bubble size is not the only factor that affects the bubble velocity. In churn-turbulent flow, it is not even the decisive factor. Therefore, the bubble velocity increases with bubble size and it is much higher in churn-turbulent flow than in bubbly flow. It is noteworthy that we measured chord length, not bubble size, and the relationship between bubble velocity and chord length could be more complex than that between bubble velocity and size. It is evident that in churn-turbulent flow, the velocity of a portion of small chord length bubbles is as high as that for large bubbles (Figure 12d). This implies that the high velocity at small chord lengths is not necessarily due to small bubbles, but may be caused by large bubbles pierced at the side. In addition, many small bubbles exist in the wake of large bubbles and they move with the large bubbles. In a few cases, large bubbles have relatively low velocity. One possible reason is that large bubbles tend to vibrate seriously during movement, and if the probe hits the part of a large bubble that is vibrating in the opposite direction to the bubble velocity vector, then the velocity detected by the probe will be much lower than the real velocity of the bubble. Besides, the flow field in bubble columns is very complicated and it can affect the bubble velocity significantly. For example, a down flow liq-

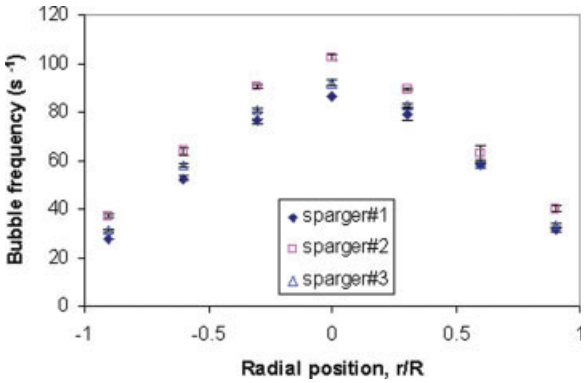

Figure 13. Sparger effect on bubble frequency in the sparger zone (z/D = 1.7, U_g = 30 cm/s).

[Color figure can be viewed in the online issue, which is available at www.interscience.wiley.com.]

uid stream can temporarily decrease the velocity of some large bubbles. If such liquid down draft occurs locally at the time of large bubble arrival at the probe top, the bubble velocity lower than expected based on its chord length will be detected.

The effect of spargers

It has been reported that the configuration of the sparger, for example, the number and size of the orifices, affects the generation of bubbles and subsequently may affect the hydrodynamics in bubble columns.[10–12] As shown in Figure 4 and detailed in Table 2, three spargers were used in this study: a cross sparger (Sparger No. 1), a perforated plate with 0.15% open area (Sparger No. 2), and a perforated plate with 1.0% open area (Sparger No. 3).

It was found that, in the sparger zone (z/D = 1.7), at fixed superficial gas velocity the bubble frequency increased in the order of Sparger No. 1, Sparger No. 3, and Sparger No. 2, as shown in Figure 13. Sparger No. 1 and No. 3, which are totally different in their hole numbers, hole sizes, and hole distributions, generate bubbles of relatively similar properties, for example, bubble frequency.

Figure 14 shows the bubble chord length distributions in the column center in the sparger zone (z/D = 1.7) for the three spargers. The distributions for Sparger No. 1 and No. 3 are again alike except for the fact that Sparger No. 3 produced an additional peak at small values of bubble chord length. The bubble chord length distribution for Sparger No. 2 has a higher probability density at small values of chord length. The mean bubble chord length and standard deviation of the bubble

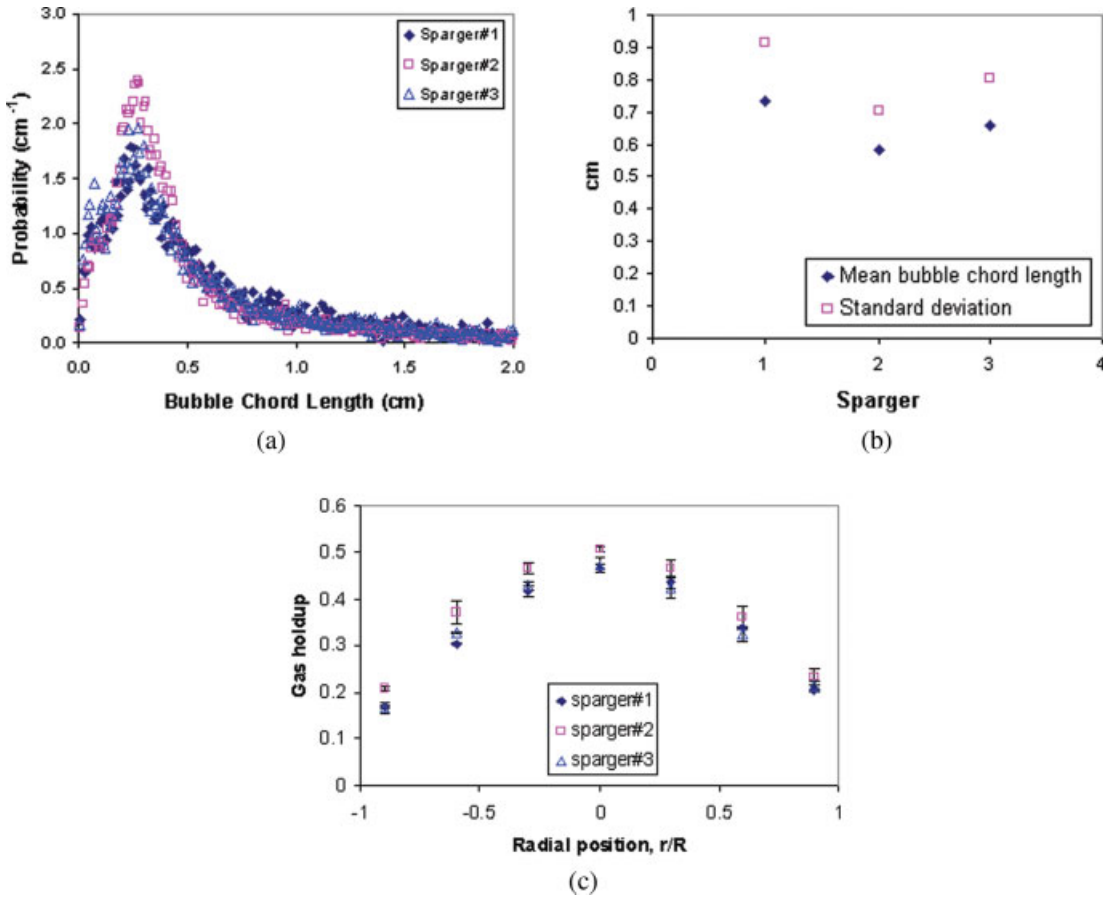

Figure 14. Sparger effect on (a) bubble chord length distribution, (b) mean bubble chord length, and (c) local gas holdup (30 cm/s, z/D = 1.7, r/R = 0).

[Color figure can be viewed in the online issue, which is available at www.interscience.wiley.com.]

Table 3. Comparison of the Predicted Initial Bubble Size and Mean Bubble Chord Length Obtained by the Four-Point Optical Probe

Sparger	P (MPa)	U_g (cm/s)	Initial Bubble Size (cm)			Mean Chord Length by Probe* (cm)	
			Ellenberger and Krishna[13]	Leibson et al.[14]	Wallis[15]	$r/R = 0$	$r/R = -0.9$
1	0.1	30	14.3	0.41	0.52	0.731	0.357
2	0.1	30	3.25	0.42	0.1	0.582	0.265
3	0.1	30	3.25	0.48	0.25	0.659	0.368

*In the sparger zone, $z/D = 1.7$.

chord length distributions decreases in the order of Sparger No. 1, Sparger No. 3, and Sparger No. 2 (Figure 14b). Consequently, the local gas holdup at $z/D = 1.7$ increases in the same order, that is, Sparger No. 2 produced the highest local gas holdup and Sparger No. 1 and No. 3 gave almost the same gas holdup, as shown in Figure 14c.

Some correlations have been developed for the estimation of the initial bubble size at the sparger.[13–15] The estimated initial bubble sizes based on these predictions are listed in Table 3.[3] Obviously, the initial bubble size by the prediction of Ellenberger and Krishna[13] is too large. The initial bubble sizes predicted by Leibson et al.[14] and Wallis[15] are of the same order of magnitude as the mean bubble chord length obtained by the four-point probe. Although the bubble size increases with axial position in the sparger zone due to bubble coalescence so that the bubble size at the measuring position of the probe ($z/D = 1.7$) is larger than at the sparger, the bubble size predicted by the proposition of Wallis[15] for

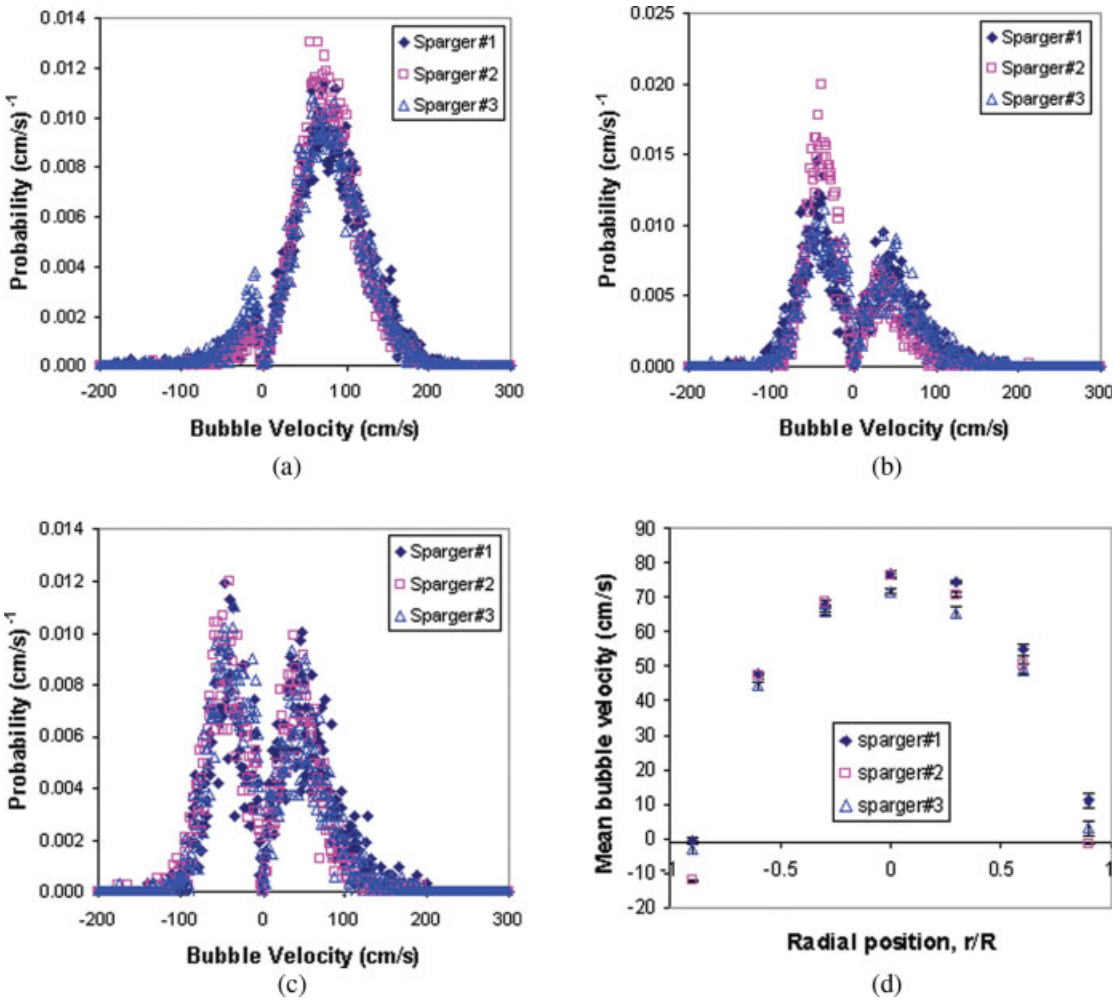

Figure 15. Sparger effect on bubble velocity distribution and mean bubble velocity (30 cm/s, $z/D = 1.7$).

(a) $r/R = 0$; (b) $r/R = -0.9$; (c) $r/R = 0.9$; (d) mean bubble velocity. [Color figure can be viewed in the online issue, which is available at www.interscience.wiley.com.]

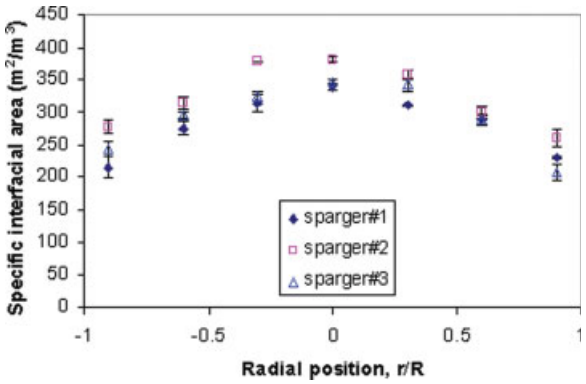

Figure 16. Sparger effect on specific interfacial area (30 cm/s, $z/D = 1.7$).

[Color figure can be viewed in the online issue, which is available at www.interscience.wiley.com.]

Sparger No. 2 and No. 3 still seems to be too small. Furthermore, the initial bubble size increases in the order of Sparger No. 1, No. 2, and No. 3 according to the prediction of Leibson et al.,[14] whereas the mean bubble chord length obtained by the probe ($r/R = 0$) increases in the order of Sparger No. 2, No. 3, and No. 1. Hence, the initial bubble size estimated by these predictions does not fit the experimental results in this study very well.

The bubble velocity distributions in the sparger zone for different spargers are shown in Figure 15. It was found that Sparger No. 1 and No. 3 generated approximately the same bubble velocity distribution at different radial positions in the sparger zone (Figures 15a–c). Sparger No. 2 generated more bubbles moving downward in the wall zone, especially at $r/R = -0.9$ (Figure 15b). This is also clear from the radial profiles of the mean bubble velocity for different spargers (Figure 15d), where it can be seen that, for the three spargers used, the mean bubble velocity for sparger No. 2 is the smallest in the wall zone.

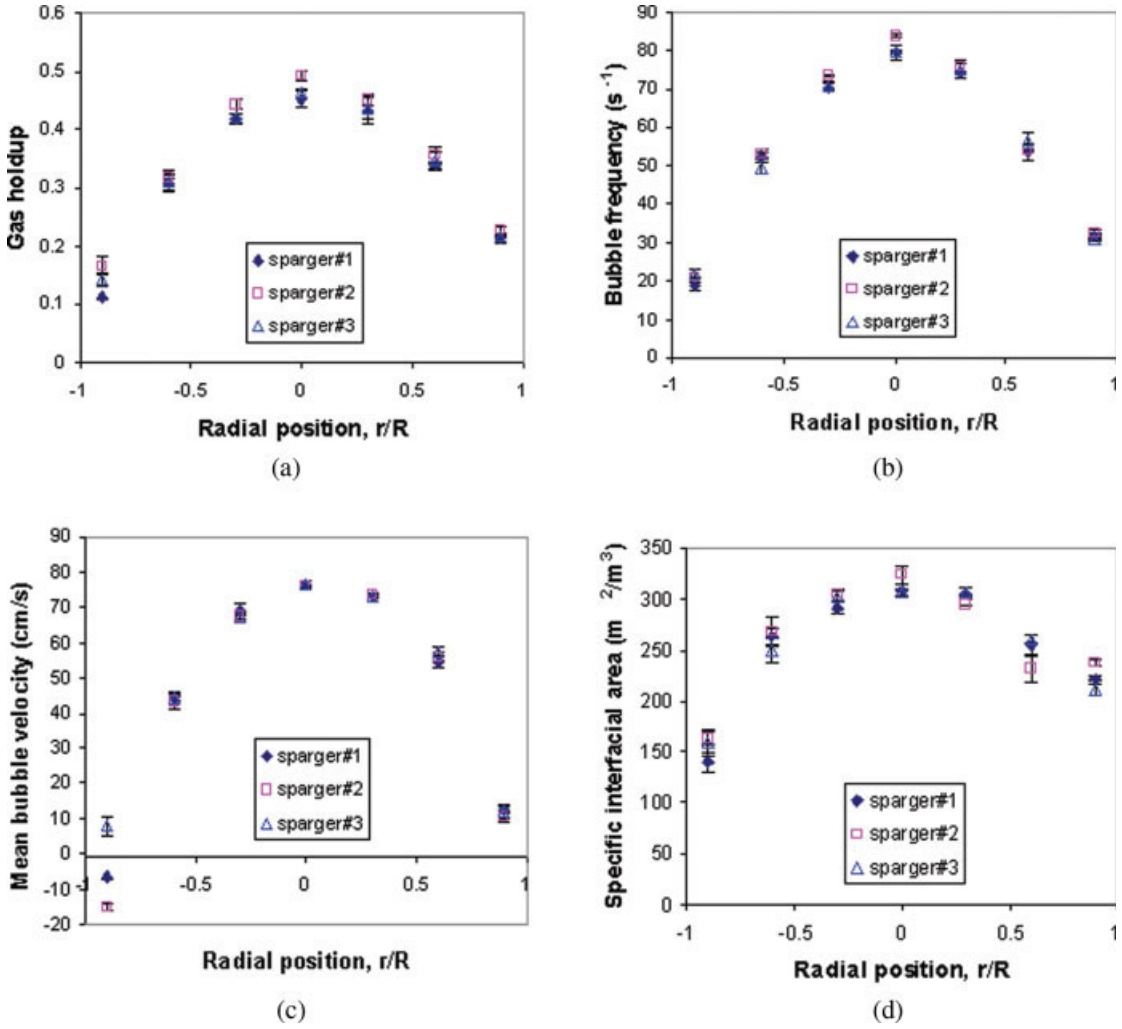

Figure 17. Bubble properties at $z/D = 5.1$ for different spargers.

(a) Gas holdup; (b) bubble frequency; (c) mean bubble velocity; (d) specific interfacial area. [Color figure can be viewed in the online issue, which is available at www.interscience.wiley.com.]

Sparger No. 2 also produced a higher specific interfacial area in the sparger zone than the other two spargers, as shown in Figure 16. This is in agreement with the radial profiles of the local gas holdup (Figure 14c) and bubble frequency (Figure 13), due to the correlation of these three variables.

Earlier by γ ray CT and CARPT experiments, Ong[3] found that deep in the churn-turbulent flow regime ($U_g \geq 30$ cm/s) at atmospheric pressure the effect of the sparger on the radial gas holdup profile and liquid recirculation in the fully developed region ($z/D \geq 5.5$) is minor. The sparger effect on bubble properties in the fully developed region obtained by the four-point probe is shown in Figure 17. It can be seen that at atmospheric pressure, the sparger effect on the radial profile of gas holdup, bubble frequency, mean bubble velocity, and specific interfacial area is small at $z/D = 5.1$. The exception is noted in the wall zone for mean bubble velocity and may be caused by the existence of coherent structures,[5] which makes the flow field in the wall zone asymmetric and causes frequent changes in the flow direction. In other words, the radial profiles of the bubble frequency, the mean bubble velocity, and the specific interfacial area for the three spargers follow the same trend as the gas holdup profiles. Hence, the sparger effect disappeared with an increase in the axial position in the bubble column, and it was not significant at $z/D > 5.1$ in this study.

The effect of axial position on bubble properties

For the operating conditions employed in this study, the mean bubble velocity profile did not change much with axial position, except at low gas velocity ($U_g = 2$ cm/s, shown in Figure 18). At $U_g = 2$ cm/s, the mean bubble velocity in the lower zone of the bubble column ($z/D = 1.7$) was higher than that in the upper zone. This is possibly due to the large initial momentum of the bubbles jetting from the sparger and the lack of liquid recirculation at low gas velocity. This was not true when $U_g \geq 8$ cm/s, that is, in the transition and churn-turbulent region, where the mean bubble velocity in the core of the column did not change much with axial position. This means that in the transition and churn-turbulent regime the mean bubble velocity profile developed very fast in the axial direction; in other words, the sparger zone for the mean bubble velocity profile is small. In the wall zone, the mean bubble velocity was different at different axial positions in both bubbly flow and churn-turbulent flow. This was due to the complexity of the flow field (i.e., the flow direction changed with time) and due to the existence of flow cells.[5]

Conclusions

The four-point optical probe performed efficiently both in bubbly flow and in highly churn-turbulent flow. Bubble properties (local gas holdup, chord length, velocity, specific interfacial area, and frequency) at these conditions in a 6.4-in. diameter bubble column were measured for the first time.

In bubbly flow, the radial profiles of specific interfacial area, bubble frequency, and mean bubble velocity are all flat. With an increase in superficial gas velocity, U_g, these profiles

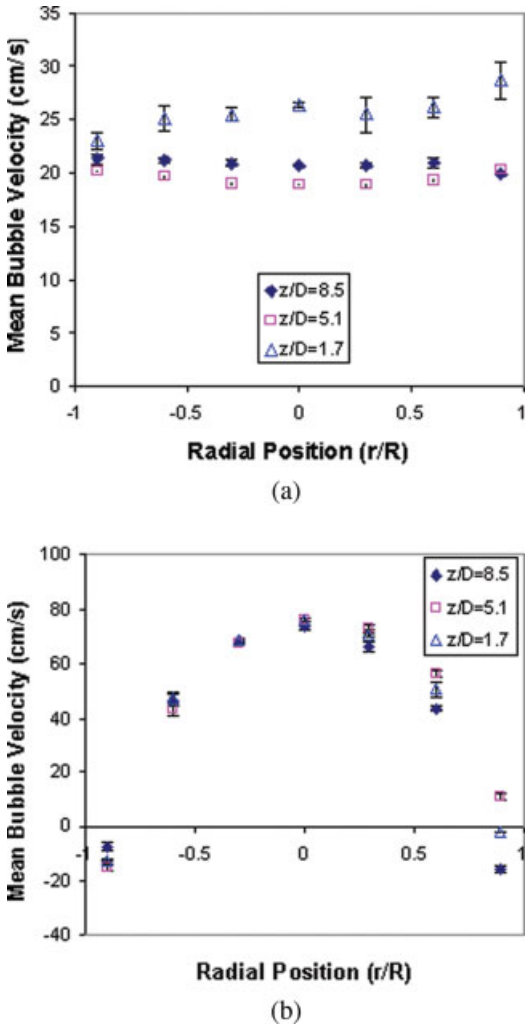

Figure 18. Mean bubble velocity profile at different axial positions (Sparger No. 2, 0.1 MPa).

(a) $U_g = 2$ cm/s; (b) $U_g = 30$ cm/s. [Color figure can be viewed in the online issue, which is available at www.interscience.wiley.com.]

became more parabolic in shape. In the column center, the bubble chord length distribution spreads wider with an increase in U_g. The mean bubble chord length increases with U_g until it is in deep churn-turbulent flow and then remains almost identical with U_g. In the wall region, the bubble chord length distribution does not change much with U_g. The mean bubble chord length in the wall region is much smaller than that in the column center, and it increases mildly with U_g between the bubbly flow and the transition flow regime, then decrease slightly with U_g.

At very low gas velocity, for example, 2 cm/s, all bubbles move upward in bubble column. In churn-turbulent flow ($U_g > 8$ cm/s), some bubbles move downward even in the column center. In the wall region, the number of bubbles moving downward is equal to or even larger than that of bubbles moving upward. The percentage of bubbles moving downward increases slowly with U_g in both the wall region and in the core of the column.

In bubbly flow, the bubble velocity distribution and bubble chord length distribution are alike at different radial positions, including in the wall region. In churn-turbulent flow, in the core of the column the bubble velocity and chord length distributions are alike at different radial position, but in the wall region they are very different from the core of the column.

Two of the three spargers used in this study, that is, Sparger No. 1 and No. 3, generated similar bubble properties at the operating conditions employed, although their configurations are totally different. Sparger No. 2 generates somewhat different bubble properties than the other two spargers, though not to a significant extent. The sparger effect disappears with an increase in the axial position in bubble column at $z/D > 5.1$.

Acknowledgments

The authors from CREL–WUSTL acknowledge the financial support provided by DOE (FC 2295 PC 95051), CREL industrial sponsors, and NSF–CEBC (NSF EEC 03106891), which made this work possible.

Literature Cited

1. Xue J, Al-Dahhan M, Dudukovic MP, Mudde RF. Bubble dynamics measurements using four-point optical probe. *Can J Chem Eng*. 2003;81:375–381.
2. Xue J. *Bubble Velocity, Size and Interfacial Area Measurement in Bubble Columns*. PhD dissertation. St. Louis: Washington University, 2004.
3. Ong B. *Experimental Investigation of Bubble Column Hydrodynamics: Effect of Elevated Pressure and Superficial Gas Velocity*. PhD dissertation. St. Louis: Washington University, 2003.
4. Kemoun A, Ong B, Gupta P, Al-Dahhan M, Dudukovic MP. Gas holdup in bubble columns at elevated pressure via computed tomography. *Int J Multiphase Flow*. 2001;27:929–946.
5. Groen JS, Oldeman RGC, Mudde RF, Van der Akker HEA. Coherent structures and axial dispersion in bubble column reactors. *Chem Eng Sci*. 1996;51:2511–2520.
6. Kataoka I, Ishii M, Serizawa A. Local formulation and measurements of interfacial area concentration in two-phase flow. *Int J Multiphase flow*. 1986;12:505–529.
7. Chen RC, Reese J, Fan LS. Flow structure in a three-dimensional bubble column and three-phase fluidized bed. *AIChE J*. 1994;40: 1093–1104.
8. Mudde RF, Groen JS, Van den Akker HEA. Liquid velocity field in a bubble column: LDA experiments. *Chem Eng Sci*. 1997;52:4217–4224.
9. Mudde RF, Saito T. Hydrodynamic similarities between bubble column and bubbly pipe flow. *J Fluid Mech*. 2001;437:203–228.
10. LaNauze RD, Harris IJ. Gas bubble formation at elevated system pressures. *Trans Inst Chem Eng*. 1974;52:337–348.
11. Idogawa K, Ikeda K, Fukuda T, Morooka S. Formation and flow of gas bubbles in a pressurized bubble column with a single orifice or nozzle gas distributor. *Chem Eng Commun*. 1987;59:201–212.
12. Terasaka K, Hieda Y, Tsuge H. SO_2 bubble formation from an orifice submerged in water. *J Chem Eng Jpn*. 1999;32:472–479.
13. Ellenberger J, Krishna R. A unified approach to the scale-up of gas–solid fluidized bed and gas–liquid bubble column reactors. *Chem Eng Sci*. 1994;49:5391–5411.
14. Leibson I, Holcomb EG, Cacoso AG, Jacmic JJ. Rate of flow and mechanics of bubble formation from single submerged orifices. *AIChE J*. 1956;2:296–306.
15. Wallis GB. *One-Dimensional Two-Phase Flow*. New York: McGraw Hill, 1969.

Manuscript received May 15, 2007, and revision received Oct. 8, 2007.